Anomalies of moment of inertia in $^{170\text{-}180}$Os

1993 J. Phys. G: Nucl. Part. Phys. 19 299

(http://iopscience.iop.org/0954-3899/19/2/012)

J. Phys. G: Nucl. Part. Phys. 19 (1993) 299–305. Printed in the UK

Anomalies of moment of inertia in $^{170-180}$Os

H C Chiang†, S T Hsieh†, M M King Yen‡ and D S Chuu§

† Department of Physics, National Tsing Hua University, Hsinchu, Taiwan, Republic of China

‡ Department of Nuclear Engineering, National Tsing Hua University, Hsinchu, Taiwan, Republic of China

§ Department of Electrophysics, National Chiao Tung University, Hsinchu, Taiwan, Republic of China

Received 29 January 1992, in final form 28 September 1992

Abstract. The anomalies of moment of inertia in $^{170-180}$Os are analysed in the interacting-boson-plus-fermion-pair model. The angular momentum–angular momentum interaction term $(\hat{L}\cdot\hat{L})$ in the boson Hamiltonian is renormalized by a $(1+f\hat{L}\cdot\hat{L})^{-1}$ factor. It was found that the renormalization facilitates the interaction parameter searching and all boson–boson and boson–fermion interaction parameters for the isotope chain can be unified. Energy levels can be reproduced quite well. The general features in the moment of inertia anomalies can be reproduced. The transition quadrupole moments are calculated and compared with other estimates.

In recent years the phenomena of shape evolution and moment of inertia anomaly have created considerable interest in nuclear structure studies. The light-mass osmium isotopes are among the nuclei which are rich in these phenomena and are suitable for comprehensive experimental and theoretical studies. Therefore, the light-mass osmium isotopes had been studied in detail in the past decade (Durell *et al* 1982, Gasson *et al* 1987, Dracoulis *et al* 1982, Neskakis *et al* 1982, Lieder *et al* 1988). Theoretical models such as the cranked-shell model, the rotating Bardeen–Cooper–Schrieffer model and the rotor-plus-quasiparticle model were used to analyse the complicated nuclear structure of the osmium isotopes. A systematic study of the even–even osmium isotopes with mass number 172–180 were carried out in the framework of interacting-boson-plus-fermion-pair model (Hsieh *et al* 1988). Two fermions which occupy either the $h_{9/2}$ or the $i_{13/2}$ orbital were coupled with the boson core and the moment of inertia anomalies were interpreted as the band crossings of the ground state bands and the pair aligned rotational bands. The general features of the backbending anomalies could be reproduced. The energy levels could be reproduced quite well in general except for a few states with very high spins. Quite recently, the neutron deficient osmium isotopes ^{170}Os and ^{172}Os were studied in more details (Dracoulis *et al* 1988, Wells *et al* 1989). Both experimental and theoretical studies indicate the possibility of quite complicated band crossing for the two isotopes. The isotope ^{170}Os was not included in the calculation of Hsieh *et al* owing to the lack of experimental data at that time. Therefore, it is interesting to see whether this isotope can be correlated in the IBA-plus-fermion-pair model.

In order to treat the spin dependence of the moment of inertia in the interacting

0954-3899/93/020299 + 07 $07.50

boson model Yoshida *et al* (1991) suggested a renormalization in the $\hat{L}\cdot\hat{L}$ ($\hat{L}$ being the angular momentum operator) term of the IBA Hamiltonian. A factor $1+f\hat{L}\cdot\hat{L}$ (f being a constant) is added to the denominator of the $\hat{L}\cdot\hat{L}$ term. The inclusion of this factor has the effect of suppressing the calculated energies of the high-spin states. A phenomenological calculation was performed on ^{160,164}Er and dramatic improvements in the energy level fittings were obtained. This renormalization using the factor $(1+f\hat{L}\cdot\hat{L})^{-1}$ was interpreted microscopically as the anti-pairing effect in the high-spin region. Therefore, in the analyses of high spin anomalies it is suitable to take this into account. Also, in phenomenological calculations, it is interested to see the effect of this factor in the optimization of interacting parameters.

In this work, we introduce the renormalization factor in the boson-plus-fermion-pair model (Yoshida *et al* 1982, Hsieh and Chuu 1987, King Yen *et al* 1988). This model space includes two types of basis states:

$$|n_s n_d v r\rangle_I \qquad \text{and} \qquad |n_s' n_d' v' r' L_B; j^2 J\rangle_I.$$

Here n_s (n_s'), n_d(n_d') are the numbers of s- and d-bosons, $n_s+n_d=n_s'+n_d'+1=N_B$, where N_B is the total number of bosons. The j which denotes the fermion orbital angular momentum can assume the value $\frac{13}{2}(i_{13/2})$ or $\frac{9}{2}(h_{9/2})$. $j=\frac{13}{2}$ is chosen since the $\nu(\frac{13}{2})^2$ alignment plays an important role in the high-spin anomalies in this region. Also, since the proton $h_{9/2}[541]\frac{1}{2}$ orbit gets low and lies near to the fermi levels of the Os isotopes under consideration (Rao *et al* 1986), the $\pi(h_{9/2})$ alignment will also be important. Therefore, the case with $j=\frac{9}{2}$ is also included. The total angular momentum J of the fermion pair assumes the values $4, 6, 8, \ldots$ up to $(2j-1)$. The $J=0$ and 2 fermion-pair states are omitted to avoid double counting. (Yoshida and Arima 1985). The v, r (v', r') stand for the additional quantum numbers which are needed to specify a given boson state. The boson–fermion combined model space as described is too massive. In order to make the calculation feasible we have to make some truncation on the model space. Since for each value of L we need only to calculate the first few low-energy states, we couple the lowest energy states in both fermion and boson subspaces to form the total model space. To be more specific, for a given value of I we select all possible values of L_B up to I (or $2n_d'$ if $I>2n_d'$) to couple with the lowest two values of J; n compatible with the angular momentum coupling rules. For example, for $I=14$ the boson–fermion pair model includes the basis states with $L_B=2$, $J=12$ (for $j=\frac{13}{2}$); $L_B=4$, $J=10, 12$ (for $j=\frac{13}{2}$); $L_B=6$, $J=8$ (for $j=\frac{13}{2}$ and $\frac{9}{2}$) and $J=10$ (for $j=\frac{13}{2}$), etc. Since the excitation energies for the boson state increase quite rapidly as L_B goes to higher values, so the low-L_B, high-J basis states are, in fact, the most important ones. The truncated high-L_B, high-J basis states will usually produce very high excitation energy states and can be omitted. This justifies the choice of the truncation scheme.

The Hamiltonian adopted is as follows:

$$H = H_B + H_F + V_{BF}$$

where

$$H_B = \varepsilon_d d^\dagger\cdot\tilde{d} + a_1 p^\dagger\cdot p + \frac{a_2\hat{L}\cdot\hat{L}}{1+f\hat{L}\cdot\hat{L}} + a_3\hat{Q}\cdot\hat{Q}$$

is adopted from Yoshida *et al* (1991);

$$H_F = \varepsilon_j(2j+1)^{1/2}[a_j^\dagger\times\tilde{a}_j]^{(0)} + \tfrac{1}{2}\sum_J V^J(2J+1)^{1/2}[(a_j^\dagger\times a_j^\dagger)^J\times(\tilde{a}_j\times\tilde{a}_j)^J]^{(0)}$$

which includes the one-body and two-body fermion energies;

$$V_{BF} = \alpha \hat{Q} \cdot (a_j^\dagger \times \tilde{a}_j)^{(2)} + \beta \hat{Q} \cdot [(a_j^\dagger \times a_j^\dagger)^{(4)} \times \hat{d} - d^\dagger \times (\tilde{a}_j \times \tilde{a}_j)^{(4)}]^{(2)}$$

where $\hat{Q}$ is the $SU(3)$ generator quadrupole operator and equals $(d^\dagger \times s + s \times \tilde{d})^{(2)} - \frac{1}{2}\sqrt{7}\,(d^\dagger \times \tilde{d})^{(2)}$. The fermion–fermion interaction strength V^Js are calculated from the Yukawa potential with the Rosenfeld mixture. The oscillation constant ν is chosen to be $0.96A^{-1/3} \times 10^{22}\,s^{-1}$ with $A = 175$. The overall strength normalization of V^Js is determined by requiring

$$\langle jj|\,V\,|jj\rangle_2 - \langle jj|\,V\,|jj\rangle_0 = 2\,\text{MeV}.$$

The whole Hamiltonian is then diagonalized in the selected model space. The boson parameters ε_d, a_1, a_2, a_3, f, the fermion single-particle energies $\varepsilon_{9/2}$, $\varepsilon_{13/2}$ and the boson–fermion coupling parameters α, β are determined by least-squares fittings between the calculated and experimental energy levels of $^{170-180}$Os.

Since we include the renormalizations in the $\hat{L} \cdot \hat{L}$ term, it appears that we have introduced one more parameter in the IBA-plus-fermion-pair model. However, by introducing this parameter in the calculation, it was found that the determinations of other parameter become easier. In fact, it was found that the boson parameters ε_d, a_1, a_2, a_3, f and boson–fermion coupling parameters α, β could be unified for the whole $^{170-180}$Os isotope chain. Note that in the previous calculation of Hsieh *et al* (1988) mass dependent values of a_1 and a_2 were used so the number of parameters in this work is in fact reduced considerably. The values (all in MeV) $\varepsilon_d = 0.475$, $a_1 = 0.0275$, $a_2 = 0.0080$, $a_3 = -0.0066$, $f = 0.05$, $\alpha = 0.037$ and $\beta = 0.021$ are adopted for all $^{170-180}$Os isotopes. Mass dependent single-fermion energies are adopted and their values are shown in table 1. As shown in table 1, the values of $\varepsilon_{9/2}$ are lower than those of $\varepsilon_{13/2}$ and have a stronger mass dependence. In the calculation it was found that the highest spin states for each Os isotope are usually dominated by the boson plus $(i_{13/2})^2$ fermion pair configurations. On the other hand, the intermediately high-spin states and some low-spin quasi β-band or γ-band states are dominated by boson plus $(h_{9/2})^2$ fermion pair configurations. Since the properties of these states usually depend on the fine features of deformations, we expect a stronger mass dependence of $\varepsilon_{9/2}$. Also, the higher values of $\varepsilon_{13/2}$ are consistent with the states dominance of high-spin states.

The energy levels can be reproduced quite well in general. In figures 1 and 2 the calculated and experimental energy levels of ^{170}Os and ^{180}Os are shown as illustrations. The energy levels of other isotopes show similar agreement. In figure 2, two sets of calculated energy levels are shown. Both the energy levels calculated in this work (denoted as cal. A) and those obtained in Hsieh *et al* (1988) (denoted as cal. B) are compared with the experimental data. In the low-spin region the agreements between cal. A and the experimental data is only slightly better than that of cal. B. However, significant improvement is obtained in the very-high-spin region. This is, of course, related to the suppression of the high-spin state energies

Table 1. The adopted fermion single-particle energies

Nucleus	^{170}Os	^{172}Os	^{174}Os	^{176}Os	^{178}Os	^{180}Os
$\varepsilon_{9/2}$(MeV)	1.260	0.920	0.686	0.724	0.820	0.868
$\varepsilon_{13/2}$(MeV)	1.388	1.302	1.185	1.322	1.339	1.236

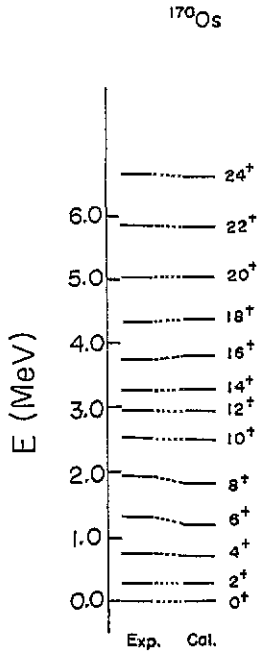

Figure 1. The calculated and experimental energy levels for ^{170}Os.

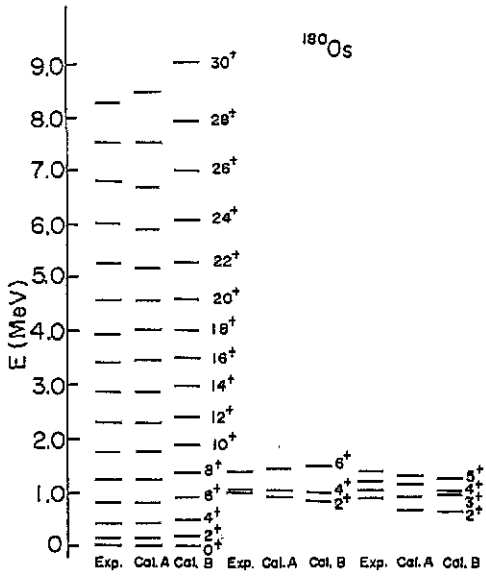

Figure 2. The calculated and experimental energy levels for ^{180}Os.

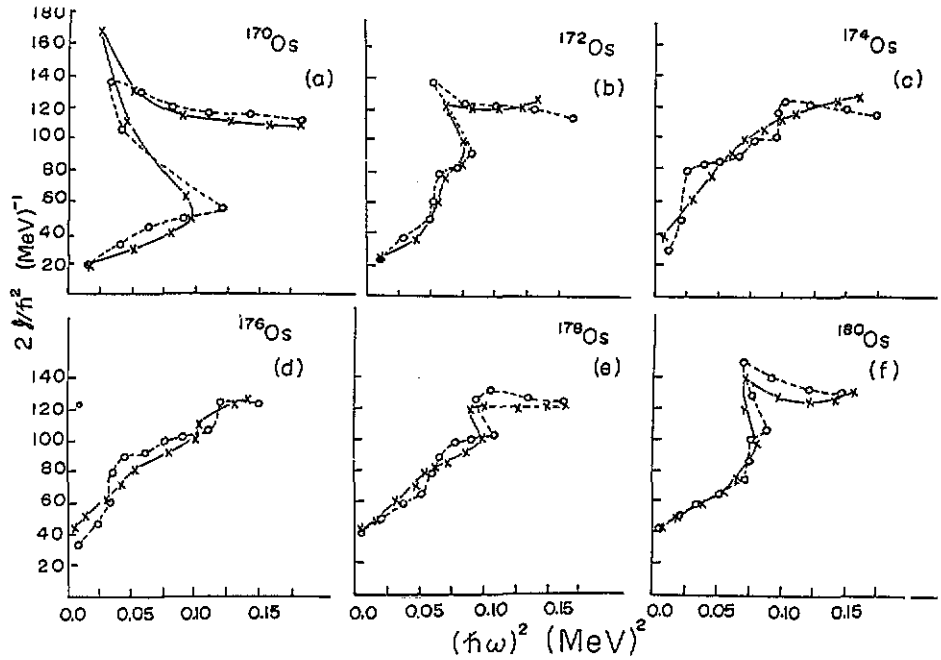

Figure 3. The backbending plot for $^{170-180}$Os. The experimental data are connected by solid curves and the calculated values are connected by dashed curves.

due to the factor $(1+f\hat{L}\cdot\hat{L})^{-1}$. Note that all boson related parameters are unified for the Os isotopes under consideration. The number of parameters in cal. A is much smaller than that of cal. B so the improvement in the energy level fittings is really a remarkable result.

For the light-mass Os isotopes the gains in the aligned angular momentum are usually plotted versus the rotational frequency (Bengtsson and Frauendorf 1979). In this work we show the conventional $2\mathcal{J}/\hbar^2$ (defined as $(4I-2)/(E_I-E_{I-2})$) versus $(\hbar\omega)^2$ (defined as $(E_I-E_{I-2})^2/\{[I(I+1)]^{1/2}-[(I-2)(I-1)]^{1/2}\}^2$) plot which is more sensitive to the moment of inertia anomalies. The corresponding curves, usually called backbending plots, for $^{170-180}Os$ are shown in figure 3. In general, the backbending behaviour can be reproduced reasonably well. Comparing the plots for the whole isotope chain it appears that the backbending features are more prominent at both the lower- and higher-mass ends. For ^{174}Os and ^{176}Os the experimental curves show relatively smooth variation as compared with the calculated curves. Both calculated curves have two upbends around $(\hbar\omega)^2\simeq 0.025\,\mathrm{MeV}^2$ and $0.11\,\mathrm{MeV}^2$. It is generally believed that the smooth increase of experimental values of $2\mathcal{J}/\hbar^2$ versus $(\hbar\omega)^2$ is a smeared manifestation of complicated band crossings. The calculation in this work which is a simplified three-band-mixing model is not expected to reproduce the details of the interplays of the mixing bands.

The analyses of wavefunctions can give us information about the positions of band crossings. The spins and their corresponding calculated excitation energies for which the $(h_{9/2})^2$ and $(i_{13/2})^2$ band configurations begin to cross the ground state bands are shown in table 2. From the table, several interesting features are worth mentioning: (i) For ^{170}Os, the $(i_{13/2})^2$ band crossing happens at relatively lower energy and spin. It was found that the $h_{9/2}$ single-particle orbital did not come into play and a two-band description is sufficient. This is consistent with the analysis by Dracoulis *et al* (1988) although it was also shown in the same reference that a three-band-mixing model produced a slightly better theory–experiment fit. For the other Os isotopes it was found that both $(h_{9/2})^2$ and $(i_{13/2})^2$ band crossing happen. (ii) For ^{172}Os and ^{180}Os the two crossing positions are closer together than those of the

Table 2. The positions of the crossing spins and energies for the $\pi(h_{9/2})^2$ and $\nu(i_{13/2})^2$ bands

Nucleus	^{170}Os	^{172}Os	^{174}Os	^{176}Os	^{178}Os	^{180}Os
$h_{9/2}$ crossing spin (I)	—	10	6	8	10	10
$h_{9/2}$ crossing energy (MeV)	—	0.241	0.134	0.186	0.243	0.267
$i_{13/2}$ crossing spin (I)	12	14	18	20	20	18
$i_{13/2}$ crossing (MeV)	0.215	0.296	0.298	0.353	0.307	0.274

other isotopes. The calculated positions are consistent with the analyses in experimental data. Note the backbending plots of ^{172}Os and ^{180}Os (figures 3(b) and 3(f)) are rather similar. (iii) The ^{174}Os and ^{176}Os isotopes have quite low crossing spins and energies for the $(h_{9/2})^2$ band. The $(i_{13/2})^2$ band crossings happen at relatively higher values of spin and energy. The positions of the two band crossings are well separated. The regions of crossings are indicated in the two regions of upbends in figure 3(c) and 3(d). The low-energy crossing of the $(h_{9/2})^2$ band is also consistent with the low values of the calculated single-particle energies $\varepsilon_{9/2}$ for these two isotopes.

We have calculated the $2_1^+ \rightarrow 0_1^+$ transition quadrupole moments. The E2 operator in the IBA-plus-fermion-pair model is given by

$$\boldsymbol{T}^{(2)} = e^B \boldsymbol{Q}^{(2)} + \alpha\, e^F (\boldsymbol{a}_j^\dagger \times \tilde{\boldsymbol{a}}_j)^{(2)} + \beta\, e^B [(\boldsymbol{a}_j^\dagger \times \boldsymbol{a}_j^\dagger)^{(4)} \times \tilde{\boldsymbol{d}} - \boldsymbol{d}^\dagger \times (\tilde{\boldsymbol{a}}_j \times \tilde{\boldsymbol{a}}_j)^{(4)}]^{(2)}$$

where

$$\boldsymbol{Q}^{(2)} = \boldsymbol{d}^\dagger \times \boldsymbol{s} + \boldsymbol{s}^\dagger \times \tilde{\boldsymbol{d}} + \chi(\boldsymbol{d}^\dagger \times \tilde{\boldsymbol{d}})^{(2)}.$$

The values of α and β are adopted from the Hamiltonian. It was found that the major contributions of the quadrupole moments came from the boson part and did not depend on the value of e^F sensitively. The values of e^B and e^F are chosen as 0.15 and 0.37, respectively. These values are similar to those adopted in the other IBA-plus-fermion-pair calculations (Yoshida *et al* 1982, Alonso *et al* 1988). It was also found that the mass dependence of the calculated transition quadrupole moments does not depend on the values of χ sensitively. Here, we shall report the case with $\chi = -\sqrt{7}/2$ which unifies the two $\boldsymbol{Q}$ operators appeared in $\boldsymbol{T}^{(2)}$ and the Hamiltonian. The calculated quadrupole moments are plotted in figure 4. In the figure several experimental and other theoretical estimates are also shown for comparison. Experimental data on the B(E2) values and quadrupole moments are quite meager. It seems that the values obtained in this work have a stronger mass dependence as compared with other estimates.

In summary, a three-band phenomenological IBA-plus-fermion-pair model is applied to the neutron deficient $^{170-180}$Os even isotopes. The $\hat{\boldsymbol{L}} \cdot \hat{\boldsymbol{L}}$ term in the boson Hamiltonian is renormalized by a factor $1/(1 + f\hat{\boldsymbol{L}} \cdot \hat{\boldsymbol{L}})$ to account for the spin dependence of the moment of inertia. It was found that the inclusion of such a renormalization factor could improve the theory–experiment fittings of the energy levels in the very high-spin region. Furthermore, the mass dependence in the boson Hamiltonian which is generally needed in this type of calculation can be avoided by taking this renormalization effect into account. The general features of the moment

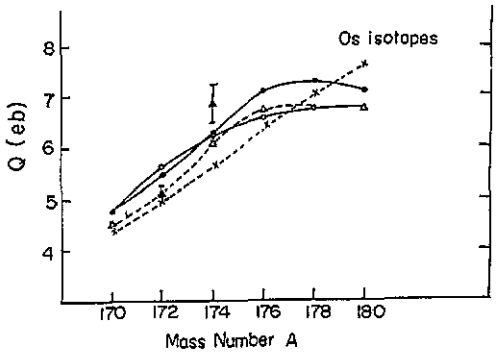

Figure 4. The comparison of the calculated quadrupole moment of this work (crosses) and other theoretical and experimental estimates. The experimental estimates are from the level energies interpreted in the variable moment of inertia model (Mariscotti *et al* 1969) (filled triangle) and the lifetime of the 2^+ states (open triangles). The theoretical estimates come from equilibrium deformation predictions given by Strutinsky-type calculations with the Nilsson potential (filled circles) and Woods–Saxon potential (open circles).

of inertia anomalies can be reproduced. The detailed analysis on the positions of crossing energies and spins indicates that these positions vary quite quickly with the change in the masses. The calculated transition quadrupole moments have a slightly steeper variation trend as compared with other theoretical and experimental estimates. An extensive comparison of the calculated $B(E2)$ values to the correponding experimental data when they are available in the future will provide a more crucial test of the model.

Acknowledgment

Research sponsored by the National Science Council of the Republic of China under the grant no NSC80-0208-M007-13.

References

Alonso C E, Arias J M and Lozano M 1986 *Phys. Lett.* B **177** 130
Bengtsson R and Frauendorf S 1979 *Nucl. Phys.* A **327** 139
Dracoulis G D, Fahlander C and Fewell M P 1982 *Nucl. Phys.* A **383** 119
Dracoulis G D, Bark R A, Stuchberg A E, Byrne A P, Baxter A M and Riese F 1988 *Nucl. Phys.* A **486** 414
Durell J L, Dracoulis G D, Fahlander C and Byrne A P 1982 *Phys. Lett.* **115B** 367
Gasson J *et al* 1987 *Nucl. Phys.* A **470** 230
Hsieh S T and Chuu D S 1987 *J. Phys. G: Nucl. Phys.* **13** L241
Hsieh S T, King Yen M M and Kuo T T S 1988 *J. Phys. G: Nucl. Phys.* **14** L31
King Yen M M, Hsieh S T and Chiang H C 1988 *Phys. Rev.* C **38** 993
Lieder R M, Neskakis A, Skalski J, Sletten G, Garrett J D and Dudek J 1988 *Nucl. Phys.* A **476** 545
Mariscotti M A J, Scharff-Goldhaber G and Buck B 1969 *Phys. Rev.* **178** 1864
Neskakis A and Lieder R M 1982 *Phys. Lett.* **18B** 49
Rao M N *et al* 1986 *Phys. Rev. Lett.* **57** 667
Wells J C *et al* 1989 *Phys. Rev.* C **40** 725
Yoshida N, Arima A and Otsuka T 1982 *Phys. Lett.* **114B** 86
Yoshida N and Arima A 1985 *Phys. Lett.* **164B** 231
Yoshida N, Sagawa H, Otsuka T and Arima A 1991 *Phys. Lett.* **256B** 129